

M-mode photoacoustic particle flow imaging

Hui Fang and Lihong V. Wang*

Optical Imaging Laboratory, Department of Biomedical Engineering, Washington University in St. Louis,
One Brookings Drive, St. Louis, Missouri 63130, USA

*Corresponding author. lhwang@biomed.wustl.edu

Received November 24, 2008; accepted December 23, 2008;
posted January 29, 2009 (Doc. ID 104498); published February 26, 2009

Recently, there has been growing interest in the development of photoacoustic flow measuring methods aimed to study microvascular blood flow in biological tissue. Here, we describe the *M*-mode photoacoustic particle flow imaging, using an optical resolution photoacoustic microscope equipped with a high-repetition-rate pulsed dye laser. We studied the flow of a diluted dyed particle suspension in a small tube embedded in a nonscattering medium as well as in a scattering medium simulating biological tissue. Potentially, the method can be applied to detect the flow speed of single red blood cells in a capillary. © 2009 Optical Society of America

OCIS codes: 170.5120, 120.7250.

For the imaging methods that have been applied to study microvascular blood flow (best known as “microcirculation”), we may categorize them into three groups based on their major principles: Doppler flow imaging [1–3], speckle contrast flow imaging [4,5], and particle imaging velocimetry (PIV) [6–8]. These methods use either light or sound as a probe. For example, laser Doppler imaging [1] and optical PIV [6] use only light, while ultrasound Doppler imaging [3] and ultrasonic echo PIV [8] use only sound. As a consequence, except fluorescent contrast PIV [7], all of the methods employ the scattering property of exogenous particles or endogenous red blood cells (RBCs) to provide the imaging contrast. However, because the tissue has a high optical scattering coefficient and the ultrasonic reflection from tissue boundaries is usually much stronger than the ultrasonic scattering from RBCs, the current methods are hampered in measuring microcirculation by limitations of sensitivity, spatial resolution, or detection depth.

Photoacoustic imaging, on the contrary, applies both light and sound to work as a probe and relies on light absorption contrast agents such as RBCs [9]. This imaging modality has been demonstrated as a powerful tool for studying microvascular structures in deep tissue [10] as well as for monitoring blood hemoglobin oxygenation in microvessels [11]. Recently, there is also growing interest in developing photoacoustic blood flow measurements [12,13]. Because of the advantage in imaging depth as well as the high photoacoustic signal contrast produced by RBCs or exogenous light-absorbing particles relative to surrounding tissue, when applied to microcirculation study, photoacoustic flow measurement is expected to be able to alleviate the hindrance of the aforementioned methods.

Previously, we have demonstrated photoacoustic Doppler flow measurement [13]. In this Letter, we report another photoacoustic flow measurement method called *M*-mode photoacoustic particle flow imaging. Here, the *M*-mode means “motion mode,” and its concept follows from the *M*-mode ultrasound imaging, which is primarily used in echocardiography [14]. As will be demonstrated, the new method can detect the flow speed perpendicular to

the ultrasonic axis, while the photoacoustic Doppler flow measurement detects only the flow speed along the ultrasonic axis.

We captured the *M*-mode photoacoustic particle images by the newly developed optical resolution photoacoustic microscope (OR-PAM) [15]. Figure 1 illustrates the imaging process. Starting from the top in the figure, a pulsed laser beam (wavelength, 570 nm; pulse repetition rate, 2 kHz; pulse duration, 7 ns; and laser energy per pulse, ~100 nJ) is focused by a microscope objective (NA = 0.1) and illuminates a flowing fluid inside a small Tygon tube. The tube (inner diameter, 0.25 mm; outer diameter, 0.76 mm; S-54-HL, Saint-Gobain Performance Plastics) was fixed horizontally inside a clear gelatin medium, which was made from the mixture of porcine gelatin powder and water with a mass ratio of 1 to 10. The fluid was created by suspending red dyed polybeads (mean diameter, 6.0 μm ; diameter standard deviation, 0.6 μm ; Polysciences, Inc) in distilled water with a particle concentration of $\phi = 0.5\%$. An appropriate amount of solid sodium polytungstate (Sometu) was added to match the fluid mass density to that of the microspheres ($\rho \approx 1.05 \text{ g/cm}^3$). The flow was created by a syringe pump (BSP-99M, Braintree Scientific) and a 1 cc syringe (Multifit, Becton, Dickinson & Co.).

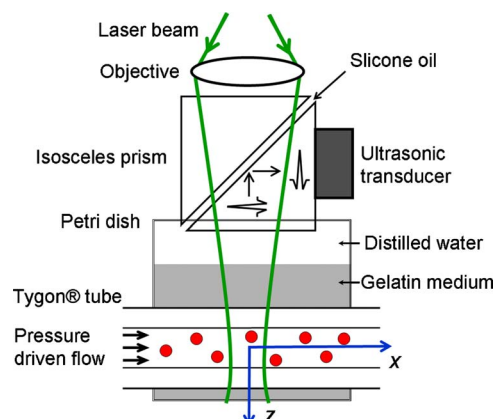


Fig. 1. (Color online) Schematic of *M*-mode photoacoustic particle imaging system.

As Fig. 1 illustrates, when a bead passes through the laser focal zone, a time sequence of photoacoustic pulses are generated and subsequently detected by an ultrasonic transducer. Here, the image is not formed by sample scanning or laser scanning. Rather, the flowing beads actually scan themselves through the laser focus. Because of using OR-PAM, the length of time during which a bead can be imaged is determined by the laser focal spot size ($\sim 5 \mu\text{m}$ in diameter) but not the ultrasonic focal spot size, which is much larger. However, the ultrasonic transducer provides an axial imaging resolution about $15 \mu\text{m}$.

As examples, in Fig. 2, two M -mode photoacoustic particle images acquired from a nonscattering background medium are presented. Figure 2(a) presents the image when the volume flow rate \dot{Q}_{Set} is set through the syringe pump as 0.04 cc/h , and Fig. 2(b) presents the image when \dot{Q}_{Set} is increased to 0.16 cc/h . The two \dot{Q}_{Set} , after being divided by the cross sectional area of the tube, correspond to the average flow speeds \bar{v}_{Set} of 0.22 mm/s and 0.88 mm/s , respectively. In the image display, the horizontal axis plots the time t , which has an interval of 0.5 ms , and the vertical axis plots the axial position z , which has a step size of $7.5 \mu\text{m}$. As shown in Fig. 2(a), there is only a single trace inside the tube, which means only one bead was imaged within the time window. However, in Fig. 2(b), four shorter traces can be seen, indicating that four beads were imaged. The dim traces located at the bottom part of both images are formed by the acoustic reflection off the tube surface.

To show the photoacoustic signal produced by the bead, Fig. 2(c) plots the A-line signal taken from the M -mode image in Fig. 2(a) at $t=200$. The photoacoustic signal generated by an incompressible sphere can be understood by the theory discussed in [16]. Fur-

thermore, to compare the profile difference between the traces in Figs. 2(a) and 2(b), Fig. 2(d) plots the M -mode signal taken from Fig. 2(a) at $z=38$ and also plots the M -mode signal taken from Fig. 2(b) at $z=43$ (across the last trace). It was determined that both of the M -mode signals fit well with Gaussian profiles. Also, Fig. 2(d) plots each signal's best fit. The fitting, under the condition of 95% confidence fit with the following Gaussian profile:

$$s(t, z) = s_0(z) \exp \left[- \frac{(t - t_0)^2}{T(z)^2} \right], \quad (1)$$

resulting in profile width $T(38) = (50.0 \pm 1.5) \times 0.5 \text{ ms}$ and $T(43) = (8.6 \pm 0.5) \times 0.5 \text{ ms}$, respectively.

The Gaussian profile of the M -mode signal, $s(t, z)$, is actually related to the laser intensity distribution and the particle geometry (Fig. 1). If the absorbing particle is infinitely small, $s(t, z)$ exactly reflects the laser intensity distribution at the depth of the particle z , which can be expressed as

$$I(x, z) = I_0(z) \exp \left[- \frac{(x - x_0)^2}{w(z)^2} \right]. \quad (2)$$

However, in the study reported here, the particle size is comparable with the laser focal spot size. Consequently, $s(t, z)$ reflects the convolution of $I(x, z)$ with the geometric profile of the particle, $p(x)$. Here, we assume that $p(x)$ also has a Gaussian shape expressed as

$$p(x) = \exp \left(- \frac{x^2}{a^2} \right), \quad (3)$$

where a is a constant related to the particle size. We therefore obtained the convolution as

$$I'(x, z) = I(x, z) \otimes p(x) = I'_0(z) \exp \left[- \frac{(x - x_0)^2}{w'(z)^2} \right], \quad (4)$$

where $w'(z)^2 = w(z)^2 + a^2$.

As time elapses from t_0 to t [see Eq. (1)], the particle at z flows from x_0 to x [as in Eq. (4)] with a speed $v(z)$. Therefore, we have $v(z) = (x - x_0)/(t - t_0)$. Finally, because $s(t, z) \propto I'(x, z)$ [16], we obtain

$$v(z) = \frac{w'(z)}{T(z)}. \quad (5)$$

To obtain $w'(z)$, we imaged the same type of polybeads through x - y two-dimensional raster scanning [15]. The sample was made by embedding the beads into the same type of clear gelatin medium as used for embedding the tube. A 3D photoacoustic image was acquired. From the image slice at each z plane, we analyzed the signal profile $I'(x, z)$ from several individual beads and obtained $w'(z)$ by the same Gaussian fitting process as that used to obtain $T(z)$. At $z=38$, $z=43$, and $z=51$ (laser focal plane), we get $w'(38) = (9.6 \pm 0.7) \times 0.625 \mu\text{m}$, $w'(43) = (6.7 \pm 0.2) \times 0.625 \mu\text{m}$, and $w'(51) = (5.9 \pm 0.2) \times 0.625 \mu\text{m}$, respectively. By using Eq. (5) and the extracted

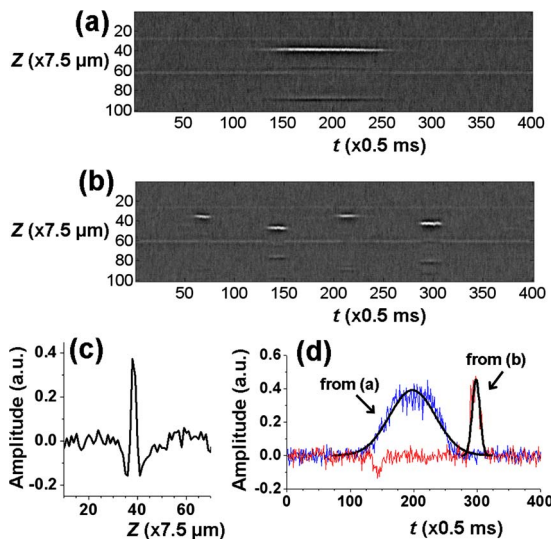


Fig. 2. (Color online) M -mode photoacoustic particle images from a nonscattering background medium. (a) M -mode image when the average flow speed is set as 0.22 mm/s . (b) M -mode image when the average flow speed is increased to 0.88 mm/s . (c) A-line signal taken from (a) at $t=200$. (d) M -mode signals taken from the images in (a) and in (b) and their Gaussian fits.

$T(38)$ and $T(43)$, finally, we obtained $v(38) = 0.24 \pm 0.02$ mm/s for the bead imaged in Fig. 2(a) and $v(43) = 0.97 \pm 0.09$ mm/s for the last bead imaged in Fig. 2(b). Both of these measured flow speeds agree with the \bar{v}_{Set} , respectively.

We applied this method to study the flow profile inside the tube as shown in Fig. 1. We studied the flow with $\bar{v}_{\text{Set}} = 0.88$ mm/s. As illustrated in Fig. 3(a), we scanned the laser beam across the cross section of the tube with a step size of $20 \mu\text{m}$. At each scanning step, we took the M -mode image with a sufficient length of time and then analyzed five particle imaging traces at the laser focal plane $z = 51$. The extracted flow speeds at each scanning step are plotted in Fig. 3(b). Considering that the resulted flow speeds at the tube center are close to $\bar{v}_{\text{Set}} = 0.88$ mm/s, as well as that the resulted flow speeds near the tube edge could be underestimated owing to a possible enlargement of the laser focus there, we observed a blunted profile despite the fact that the Reynold number is actually less than 1. The blunted profile has been previously discussed, for example, in [17] for the pressure driven flow of a particle suspension and in [6] for the blood flow in microvessels.

We also measured the flow in a scattering medium. The same type of flow as well as the same measuring geometry, as those used in the above flow profile study, were studied. In this instance, the clear gelatin medium was replaced by a scattering gelatin medium that was made by adding 20% Intralipid suspension to the gelatin solution to reach a final Intralipid concentration of 0.5%. The scattering medium has a scattering coefficient $\mu_s \approx 3 \text{ mm}^{-1}$ and a reduced scattering coefficient $\mu'_s \approx 0.7 \text{ mm}^{-1}$ at the laser wavelength according to [18]. The scattering depth, the distance from the top surface of the gelatin medium to the top outer surface of the tube [Fig. 3(a)], is $\sim 500 \mu\text{m}$. In Fig. 3(c), an M -mode signal profile measured in the scattering medium (lower thin red curve) is compared with one measured in the

clear gelatin medium. The signals, both taken at $z = 51$, were measured when the laser beam was scanned to the tube center [Fig. 3(a)]. The Gaussian fittings yield $T(51) = (7.6 \pm 1.0) \times 0.5$ ms for the lower profile and $T(51) = (7.4 \pm 0.2) \times 0.5$ ms for the taller profile, respectively. After applying in Eq. (5) the same $w'(51) = (5.9 \pm 0.2) \times 0.625 \mu\text{m}$ for both above $T(51)$, we obtained the flow speed measured in the scattering medium $v(51) = (0.97 \pm 0.16)$ mm/s and that measured in the clear gelatin medium $v(51) = (0.99 \pm 0.06)$ mm/s.

In summary, we have investigated the M -mode photoacoustic particle flow imaging. We have demonstrated its applications for studying a flow profile and for measuring the flow in a scattering medium. Potentially, this method can be applied to study microvascular blood flow in tissue. Especially, we anticipate that the method can be applied directly to measure the speed of individual RBCs in a capillary.

This research is supported by the National Institutes of Health (NIH) grants R01 EB000712 and R01 NS046214. L. V. Wang has a financial interest in Endra, Inc., which did not support this work. We acknowledge Song Hu and Konstantin Maslov for their help with the experiment.

References

1. H. Golster, M. Linden, S. Bertuglia, A. Colantuoni, G. Nisson, and Folke Sjoberg, *Microvasc. Res.* **58**, 62 (1999).
2. R. K. Wang, *Phys. Med. Biol.* **52**, 531 (2007).
3. D. E. Geortz, J. L. Yu, R. S. Kerbel, P. N. Burns, and F. S. Foster, *Ultrasound Med. Biol.* **29**, 39 (2003).
4. H. Y. Cheng, Q. M. Luo, Q. Liu, Q. Lu, H. Gong, and S. Q. Zeng, *Phys. Med. Biol.* **49**, 1347 (2004).
5. L. Sandrin, S. Manneville, and M. Fink, *Appl. Phys. Lett.* **78**, 1155 (2001).
6. Y. Sugii, S. Nishio, and K. Okamoto, *Ann. N.Y. Acad. Sci.* **972**, 331 (2002).
7. M. L. Smith, D. S. Long, E. R. Daminao, and K. Ley, *Biophys. J.* **85**, 637 (2003).
8. H. B. Kim, J. Hertzberg, C. Lanning, and R. Shandas, *Ann. Biomed. Eng.* **32**, 1067 (2004).
9. L. V. Wang, *IEEE J. Sel. Top. Quantum Electron.* **14**, 171 (2008).
10. X. D. Wang, Y. J. Pang, G. Ku, X. Y. Xie, G. Stoica, and L. V. Wang, *Nat. Biotechnol.* **21**, 803 (2003).
11. H. F. Zhang, K. Maslov, G. Stoica, and L. V. Wang, *Nat. Biotechnol.* **24**, 848 (2006).
12. P. C. Li, S. W. Huang, C. W. Wei, Y. C. Chiou, C. D. Chen, and C. R. C. Wang, *Opt. Lett.* **30**, 3341 (2005).
13. H. Fang, K. Maslov, and L. V. Wang, *Appl. Phys. Lett.* **91**, 264103 (2007).
14. S. I. Rabben, A. H. Torp, A. Stoylen, S. Slordahl, K. Bjornstad, B. O. Haugen, and B. Angelsen, *Ultrasound Med. Biol.* **26**, 287 (2000).
15. K. Maslov, H. F. Zhang, S. Hu, and L. V. Wang, *Opt. Lett.* **33**, 929 (2008).
16. G. J. Diebold, A. C. Beveridge, and T. J. Hamilton, *J. Acoust. Soc. Am.* **112**, 1780 (2002).
17. P. R. Nott and J. F. Brady, *J. Fluid Mech.* **275**, 157 (1994).
18. H. J. V. Staveren, C. J. M. Moes, J. V. Marle, S. A. Prahl, and M. J. C. V. Gemert, *Appl. Opt.* **30**, 4507 (1991).

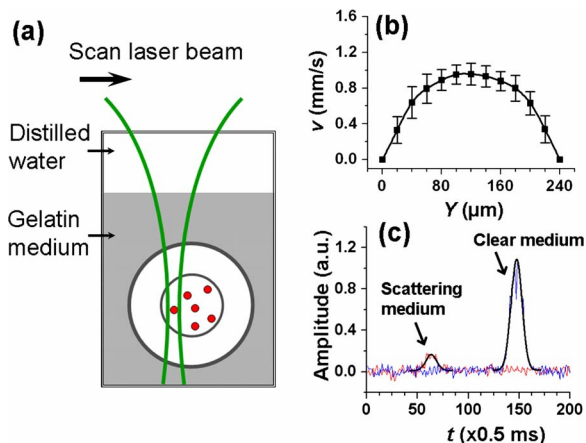


Fig. 3. (Color online) (a) Schematic of the flow profile measurement. (b) Flow profile for the average flow speed setting of 0.88 mm/s imaged from a nonscattering background medium. (c) Comparison of the M -mode signals measured in a scattering medium and a clear medium and their Gaussian fits.